Topological constraints on spiral wave dynamics in spherical geometries with inhomogeneous excitability

Jörn Davidsen,[1,2,*] Leon Glass,[3,†] and Raymond Kapral[1,2,‡]
[1]*Max-Planck-Institut für Physik Komplexer Systeme, Nöthnitzer Strasse 38, 01187 Dresden, Germany*
[2]*Chemical Physics Theory Group, Department of Chemistry, University of Toronto, Toronto, ON M5S 3H6, Canada*
[3]*Department of Physiology, McGill University, Montreal, Quebec H3G 1Y6, Canada*
(Received 29 August 2003; published 10 November 2004)

We analyze the way topological constraints and inhomogeneity in the excitability influence the dynamics of spiral waves on spheres and punctured spheres of excitable media. We generalize the definition of an index such that it characterizes not only each spiral but also each hole in punctured, oriented, compact, two-dimensional differentiable manifolds and show that the sum of the indices is conserved and zero. We also show that heterogeneity and geometry are responsible for the formation of various spiral-wave attractors, in particular pairs of spirals in which one spiral acts as a source and a second as a sink—the latter similar to an antispiral. The results provide a basis for the analysis of the propagation of waves in heterogeneous excitable media in physical and biological systems.

DOI: 10.1103/PhysRevE.70.056203 PACS number(s): 89.75.−k, 87.19.−j, 05.40.−a

I. INTRODUCTION

Geometry and inhomogeneity influence pattern formation in chemical and biological systems [1,2]. One example where these two factors play a crucial role is in the experimental observations of distinctive spiral-wave dynamics on the surfaces of spherical beads, which are excitable inhomogeneous chemical media [3,4]. A biological example is the origin of abnormal cardiac rhythms in the human heart which depend on the anatomical substrate. The heart possesses a complex nonplanar geometry with multiple chambers, with holes corresponding to valves and blood vessels. Some serious arrhythmias are associated with circulating spiral waves similar to those observed in chemical media [5]. Since an abnormal anatomical substrate is a common finding in patients with some types of cardiac arrhythmias and interventions that modify the anatomy are an accepted form of therapy [6], theoretical analyses of the interplay between geometry of the substrate and dynamics may help in the therapy of cardiac arrhythmias.

In this paper we study spiral-wave dynamics on (punctured) spheres with spatially inhomogeneous excitability. We show for punctured spheres that the sum of indices which characterize each spiral has to be zero. Moreover, we demonstrate that topological constraints imposed by the spherical geometry and inhomogeneity in excitability lead to the formation of pairs of spirals, with distinctive transient dynamics or as stable attractors, in which one spiral acts as a source and a second as a sink leading to a source-sink pair under a broad range of conditions. Our results explain the experimental observations of spirals on spherical beads [3,4]. While we do not consider detailed models of cardiac-wave propagation, our results may apply to some generic aspects of atrial arrhythmias because the thin walls of the atria can be described as two-dimensional (2D) inhomogeneous excitable media with specific geometrical features [7].

II. INDEX THEOREM FOR PHASE SINGULARITIES

The mathematical description of spiral waves is based on the notion of phase which in turn allows one to characterize spiral waves by an index. From this description, a number of topological results placing restrictions on spiral-wave dynamics can be derived [5,10–13].

With the exception of a finite number of singular points, with each point in an orientable and compact two-dimensional differentiable manifold M we identify a unique phase lying on the unit circle, $\Phi \in \mathbb{S}^1$. The resulting phase map or phase field is assumed to be continuously differentiable, except at the singular points. The manifold can be triangulated [14] (subdividing it into a set of polygons), where none of the edges or vertices of the polygons pass through a singularity. The index I (sometimes also called the topological charge or winding number) of a curve C bounding a polygon is found by computing the line integral

$$2\pi I = \oint_C \nabla \Phi \cdot d\mathbf{l}, \tag{1}$$

where the polygon is always traversed in a clockwise orientation. By continuity of $\nabla\Phi$, I must be an integer. The index of a singular point is uniquely defined as the index of any curve C provided that C encircles the point but no other singular points. The index of a curve that does not enclose any singular points is obviously zero.

If the manifold M has no boundaries, each edge of the triangulation is an edge of two polygons. Since the line integral adds up the change in phase along the various edges of the polygon, the sum of the indices of the singular points for a phase field in M is

*Electronic address: davidsen@mpipks-dresden.mpg.de
†Electronic address: glass@cnd.mcgill.ca
‡Electronic address: rkapral@chem.utoronto.ca

$$\Sigma_M I = 0, \tag{2}$$

where the sum is over all singular points. This follows since the contribution of the change in phase of each edge to the total integral is counted twice, but since the edge is traversed in opposite directions each time, the net contribution of each edge is zero. This index theorem is applicable to tori and other surfaces of genus different from 0. However, unlike the more familiar Poincaré index theorem (see Ref. [15], p. 74, for vector fields) the sum of the indices of the singular points does not depend on the genus of the surface.

This index theorem for manifolds without boundaries can be extended to manifolds with boundaries. In the following, we will consider the case of structures that arise from puncturing orientable and compact two-dimensional differentiable manifolds. The index of a hole can be uniquely defined as the index of a curve C provided that C encircles the hole but no other holes or singular points and C is positively oriented with respect to the domain which contains the hole and is bounded by C. Applying this definition and taking the summation in Eq. (2) over the singularities and the hole, or the holes if there is more than one hole, the index theorem can be proved by the same line of arguments as for the case of manifolds without boundaries.

This extension is important in the heart, for example, where the atrium is punctured by valves and veins. In such cases one is led to consider manifolds with holes—for example, a sphere with a hole. A sphere with a hole is topologically equivalent to a disk, and, indeed, the results for disks and for spheres with holes are consistent: For the disk D^2, bounded by a curve C,

$$\Sigma_{D^2} I = \oint_C \boldsymbol{\nabla}\Phi \cdot d\mathbf{l}, \tag{3}$$

so that the sum of the indices of the singular points in the disk is equal to the index of the curve C bounding the disk. If there is a single singular point on the disk, with an index of +1, the index of the curve bounding the disk will also be +1. Imagine now the boundary of the disk to be brought together (like a drawstring bag) so that the boundary of the disk now defines a hole in the sphere. In this geometry the curve C will be traversed in an opposite orientation (the hole is now inside C) from the direction it was traversed when it was the boundary of the disk. Now if there is a singular point with an index of +1 on the sphere, the index of the hole is −1, so that the sum of the indices is again zero.

Since it is necessary to conserve the sum of the indices, singularities of index ±1 usually arise and are destroyed in pairs of opposite sign [9]. An exception occurs when singularities are destroyed by collision into a boundary, so that the index of the singular point and the index of the boundary both change simultaneously. Another exception occurs if there are singularities with index different from 1. In such cases interactions between different singularities can lead to the destruction or creation of odd numbers of singularities [16].

III. FITZHUGH-NAGUMO EQUATION

The FitzHugh-Nagumo (FHN) equation [17]

$$\frac{\partial u}{\partial t} = \varepsilon^{-1}\left(-\frac{u^3}{3} + u - v\right) + D_u \nabla^2 u,$$

$$\frac{\partial v}{\partial t} = \varepsilon(u - \alpha v + \beta) + D_v \nabla^2 v, \tag{4}$$

where $u(\mathbf{r},t)$ and $v(\mathbf{r},t)$ are two scalar fields, ϵ^2 is the ratio of the time scales associated with the two fields, and D_u and D_v are the constant diffusion coefficients, is a prototypical model for excitable media. We choose $D_u=2$ and $D_v=0$. The real parameters α and β characterize the local dynamics and, hence, the local excitability. Whenever $0<\alpha<1$, $\alpha\epsilon^2<1$, and $|\beta|>\beta_H \equiv (1-\alpha\epsilon^2)^{1/2}\left[\frac{1}{3}(2\alpha+\alpha^2\epsilon^2)-1\right]$, the FHN system is excitable. At β_H a Hopf bifurcation occurs such that for $|\beta|<\beta_H$ the system exhibits oscillations. In the following we take $\alpha=0.2$, $\epsilon=0.2$, and $\beta>\beta_H=0.863\ldots$.

We consider a spherical shell whose outer and inner radii are R_e and R_i, respectively, and focus on thin spherical shells where $R_i=40$, $R_e=42$. The radii are large enough to avoid a curvature-dependent loss of excitability [18], and the shell is sufficiently thin that the dynamics is effectively 2D corresponding to the dynamics on a sphere [19]. The initial condition is a domain of an "excited" state, adjacent to a domain of the "refractory" state. Both domains have the forms of slices of the same size oriented from the north to the south pole [20] and yield a pair of counterrotating spirals.

In order to apply the topological results to the FHN equation, it is necessary to first define the phase. We define a phase, $\Phi(\mathbf{r},t)$ based on the equation $\tan\Phi(\mathbf{r},t) = v(\mathbf{r},t)/u(\mathbf{r},t)$ if $v(\mathbf{r},t)\neq 0$ and $u(\mathbf{r},t)\neq 0$. Thus, singular points at given t are points $\mathbf{r}$ in the medium for which $v(\mathbf{r},t)=0$ and $u(\mathbf{r},t)=0$. For each t, we obtain a continuously differentiable phase map $\mathcal{M}^t = \Phi(:,t)|_{\mathcal{D}^t}$ that associates to each point in a well-defined domain $\mathcal{D}^t$ a phase lying on the unit circle, $\Phi \in \mathbb{S}^1$. For our FHN medium, the domain is the surface of a (punctured) sphere reduced by a finite number of points where the phase is singular at fixed t.

Rotating spiral waves in the FHN equations are obviously associated with a singular point which is called the spiral core. In what follows, we assume that there are only single-armed spirals so that a clockwise rotating source has an index of +1 and a counterclockwise rotating source has index −1. A clockwise rotating sink has an index of −1, and a counterclockwise rotating sink has index +1. From Eq. (2), it is impossible to have a single rotating spiral wave on a sphere; in addition, there must be at least another singular point or a hole with nonzero index.

For excitable media, a nonzero index of a hole implies that wave fronts travel permanently around the hole such that the numbers of fronts traveling clockwise and counterclockwise are different. This includes the particularly simple case of a single wave front traveling around the hole which can be considered as a spiral wave associated with the hole.

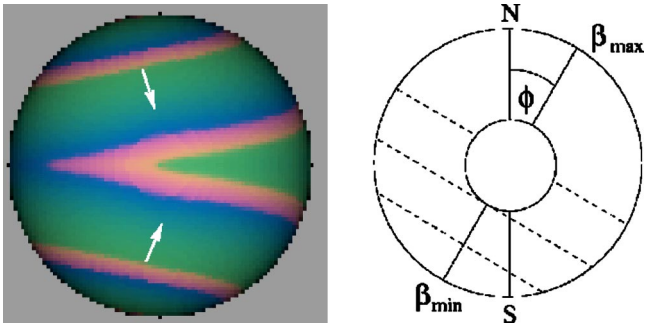

FIG. 1. (Color online) Left: spiral waves of excitation (light fronts) on the sphere for constant $\beta=\beta_{ex}$ emanating from spiral cores close to the poles on an equator projection. The white arrows show the direction of propagation. One annihilation front along the equator can be identified. Right: sketch of the constant gradient in the inhomogeneous case. The dashed lines are the equi-β lines and we choose $\beta_{max}=1.0$ and $\beta_{min}=\beta_{ex}$. The angle ϕ describes the orientation with respect to the axis from pole to pole. The results described in the text do not depend qualitatively on the choice of ϕ or β_{min} and β_{max} as long as they yield stable spirals.

IV. SPIRAL-WAVE DYNAMICS IN SPHERICAL GEOMETRIES

A. Dynamics in excitability gradients

First consider homogeneous FHN media with a constant $\beta=\beta_{ex}\equiv 0.9$. The wave fronts emanating from the spiral cores with opposite index "annihilate" along the equator such that each spiral determines the dynamics on half of the sphere (see Fig. 1, left panel)—similar to what has been observed in Ref. [21] for a different excitable system. We have shown that this behavior is robust with respect to disorder in excitability with small amplitude and correlation length. If random, uncorrelated spatial variations in β exist on length scales much smaller than the diameter of the spiral core meander [22], the dynamics is able to average over such small-scale inhomogeneities. The robustness explains why such states have been experimentally observed in some chemical reactions on spherical beads which are intrinsically inhomogeneous [4].

Applying a constant gradient in β as sketched in the right panel of Fig. 1 leads to a different scenario. The time evolution of the spiral pair may be partitioned into four distinct regimes as shown in Figs. 2 and 3. Because of the gradient, the frequencies of the two spirals differ since a higher value of β corresponds to lower excitability, which generally implies a lower spiral frequency [23]. During a short transient T, the spiral with the higher frequency assumes control of the dynamics [24] on the sphere. The location on the sphere, where wave fronts emanating from the two spiral cores annihilate, moves toward the core of the low-frequency spiral. Finally, the low-frequency spiral core is pushed farther from the high-frequency spiral core [24,25] (see Fig. 3). After this short transient, the wave fronts travel from pole to pole, leading to the creation of a source-sink pair. This (intermediate) state is shown in Fig. 4 and corresponds to regime I in Figs. 2 and 3. Viewed from the low-excitability end of the sphere, the waves wind into a small region about the core, reminiscent of the structure of antispirals—i.e., inward moving spirals seen in oscillatory media [26]. However, the origin of this inward spiral motion in oscillatory media differs and is distinct from that observed here. In oscillatory media, either spirals or antispirals are stable depending on system parameters and the wavelength diverges on the border in the parameter space between these two regimes. Thus, antispirals exist independently of spirals. This is not the case here because the generation of an inward-moving spiral relies on the presence of a spiral source and spherical geometry. For example, consider the FHN system with a disk geometry and a

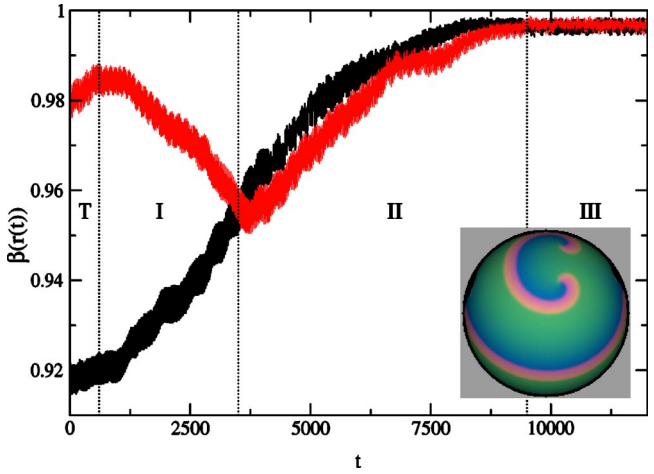

FIG. 2. (Color online) The local excitability $\beta(\mathbf{r}(t))$ at the spiral cores versus time. Gradient-induced motion of the two spiral cores leads to a change in the local excitability at the cores with time. The spiral period in the final state is $T_0=13.2\pm0.1$. Four different regimes can be identified (see text). Inset: the final bound pair of counterrotating spirals in regime III for $\phi=51.0°$ is shown on an equator projection such that the point of lowest excitability lies on the central longitude. The spiral closer to the equator has index −1 while the other one has index +1.

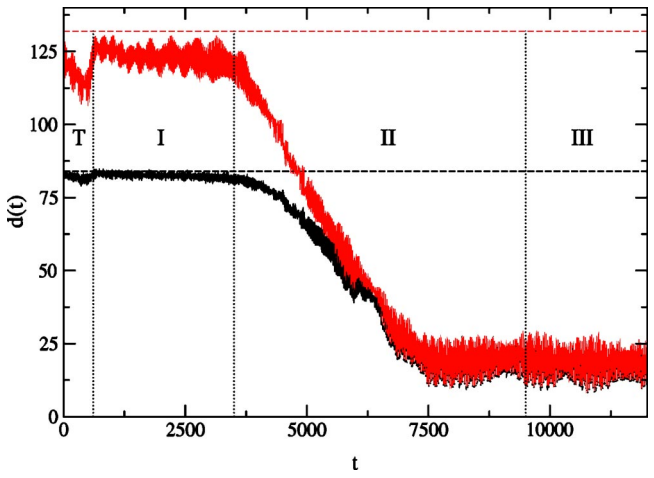

FIG. 3. (Color online) The distance between the two spiral cores $d(t)$ versus t. Gradient-induced motion of the two spiral cores leads to a change in the distance d between the cores with time. The lower and upper curves correspond to the distance in $\mathbb{R}^3$ and $\mathbb{S}^2$, respectively. The dashed lines are the respective upper bounds given by the size of the sphere.

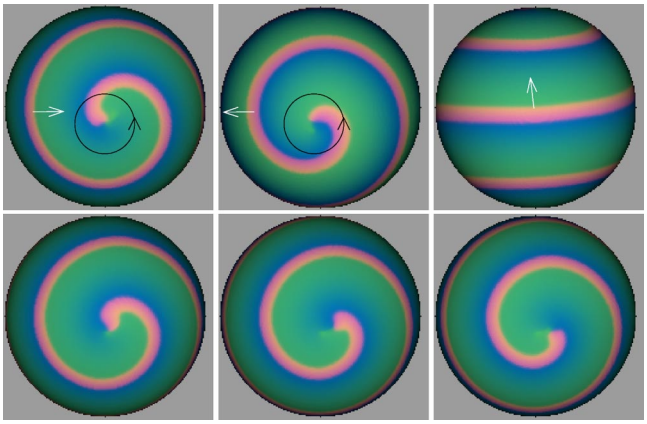

FIG. 4. (Color online) Waves of excitation on the sphere in regime I of the gradient-induced dynamics shown in Figs. 2 and 3. A source-sink pair has formed. For random spatial variations of excitability with a correlation length comparable to the diameter of the spiral core meander, the final state is very similar to the one shown here [22]. Upper panel from left to right: view centered at the north pole, south pole, and the equator. The source at the south pole has index −1 and the sink at the north pole index +1. The black circles show possible choices of C. The white arrow shows the direction of wave propagation. Lower panel: dynamics at the north pole. Time increases from left to right with $\Delta t=2.5$ between snapshots.

radial gradient in excitability such that the maximum value of β is located in the center of the disk. In this case, a source-sink pair cannot occur because the high-frequency spiral, acting as a source, would push the other (low-frequency) spiral out of the system, excluding the presence of any strong random inhomogeneities in excitability which may pin the low-frequency spiral and prevent its motion (see, e.g., [27]). The lower panel of Fig. 4 shows that remnants of the low-frequency spiral persist in a small area around the core. It has been speculated that antispiral waves might occur in cardiac tissue [28]. While excitable media cannot support a regime of exclusive antispirals due to their excitable character, our results show that source-sink pairs with similar characteristics could form in the heart where the underlying dynamics is excitable, the medium is inhomogeneous, and the topology is similar to a (punctured) sphere.

Spiral dynamics of the type described above has been observed by Maselko and Showalter [3] in experiments on the excitable Belouzov-Zhabotinsky reaction on spherical beads. They attributed the generation of spiral source-sink pairs to inhomogeneities in the medium related to differing chemical environments. This is consistent with our findings for systems with gradients and is further confirmed by the work reported in Ref. [21]. While the generation of source-sink pairs due to a gradient in the FHN medium investigated here is only an intermediate state (but one that persists for approximately 240 spiral periods in our simulations), random spatial variations of the excitability with a correlation length comparable to the diameter of the spiral core meander or larger can lead to a final state consisting of such a source-sink pair [22]. This is due to the fact that the source can be trapped in a region of depressed local excitability.

Not only does the gradient in the FHN medium change the local excitability but it also induces a drift of the spiral cores [29]. For our model, the drift is rather slow compared to the transition to the source-sink pair which takes place during the transient regime T. This can be seen in Fig. 2. [The fluctuations in $\beta(\mathbf{r}(t))$ are due to spiral meandering.] In regime I, the dominating spiral drifts toward lower excitability and its wave fronts continuously push the other core in the opposite direction, thus keeping the distance d between the cores approximately constant (see Fig. 3). The fluctuations in $d(t)$ are again due to meandering of the spiral cores. Because of this drift, the local excitabilities at the two spiral cores approach each other until they become equal.

At this point, regime II in Figs. 2 and 3 is entered. The dynamics change drastically: the enslaved spiral reverses its drift direction and regains control over its own dynamics. Both spirals drift toward lower excitability. Due to the geometric constraints imposed by the spherical geometry, the spirals approach each other until they form a bound pair (at $t\approx 7500$).

They finally reach a stable state (at $t\approx 9500$) corresponding to regime III in Figs. 2 and 3. Neither the *average* distance between the spirals nor the *average* local excitability changes further. Yet on top of the persisting unsynchronized meandering of the two spiral cores, the bound pair slowly moves along a (closed) equi-β curve on the surface of the sphere. The direction of the motion depends on the initial condition—i.e., whether the spiral with positive index was initially closer to the point of lowest excitability or to the point of highest excitability than the spiral with negative index. The wave dynamics generated by this bound pair is shown in the inset of Fig. 2.

While kinematic theory applies only to spirals with large cores, it is instructive to note that this theory predicts that the direction of the drift due to gradients depends on the model system and its parameters [30]. Although our simulations have shown the same direction of drift for a range of parameters in the meander region of the FHN phase diagram, it is conceivable that, under different circumstances favoring a drift toward higher excitability, one spiral could act as a permanent source and a source-sink pair could be the final attractor. Such a scenario would also be consistent with the experimental findings in Ref. [3].

B. Punctured spheres

Next, we consider a homogeneously excitable sphere with a single hole. Two scenarios can be observed depending on the location of the hole with respect to the spiral pair. If a spiral wave is not permanently attached to the hole, the dynamics is very similar to the case without any hole. If one of the spirals is permanently attached to the hole, the frequency of this spiral is lowered. The size of the hole determines the frequency of the spiral because the wave front has to travel around the hole. The transient dynamics is similar to that in regime T for the case with a gradient; however, no drift of the spiral cores is induced and the final state is a spiral source-sink pair as shown in Fig. 5. Not only is the net index conserved during the transition to a spiral source-sink pair

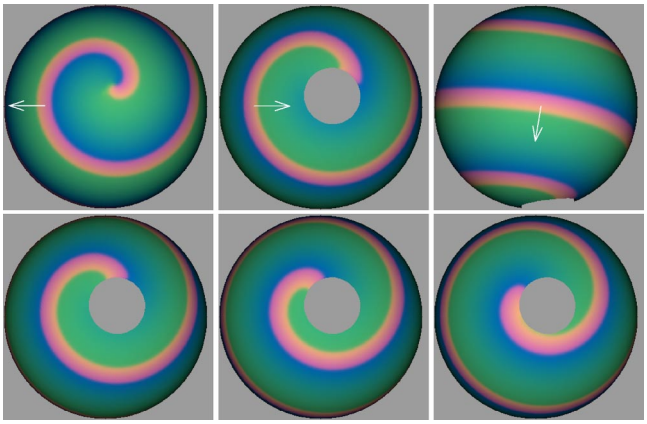

FIG. 5. (Color online) Waves of excitation on the punctured sphere propagating towards the hole. A source-sink spiral wave pair has formed in the final state. Upper panel from left to right: view centered at the north pole, south pole, and the equator. Lower panel: dynamics at the south pole. Time increases from left to right with $\Delta t = 2.5$ between snapshots.

but so is the index of the individual spirals: during the transition an outgoing-counterclockwise- (clockwise-) oriented spiral is converted into an ingoing-clockwise- (counterclockwise-) oriented spiral. Thus, the formation of spiral source-sink pairs conforms with the topological constraints.

If a gradient as well as a hole is present, the spiral drift discussed earlier also determines the final state, which depends on the hole's location in the gradient field. For instance, if the point of lowest excitability in the medium is on the hole boundary, simulations show that the spiral which is not attached to the hole will stabilize close to this point. In this final state odd numbers of wave fronts are attached to the hole, again conserving the topological charge of the hole.

V. CONCLUDING REMARKS

Inhomogeneities due to spatially varying excitability on (punctured) spherical shells lead to complex spiral-wave dynamics and the formation of source-sink spiral pairs in excitable media. The results presented here are immediately applicable to excitable media in more complicated geometries such as tori or multiholed tori and to situations in which multiarmed spirals are found. This includes mathematical modeling of cardiac tissue. The approach taken in this paper stresses constraints and aspects that apply to, and must be observed in, all realistic models of the heart satisfying certain criteria of continuity. There are also implications for the treatment of cardiac arrhythmias. In cardiology it is sometimes possible to develop maps showing the timing of the excitation over limited regions of heart [6]. In this case, a sink might be confused for a source (of the arrhythmia), and this might have implications for the diagnosis of the mechanism and the choice of therapy. The current work shows how partial knowledge about what is happening in some regions that could be observed might be helpful in establishing properties of dynamics that could not be observed. While the types of sinks we have described here have only been observed in chemical media [3,4] so far, we certainly expect their existence in the cardiological domain.

ACKNOWLEDGMENTS

We thank F. Chavez, M. Bär, S. G. Whittington, and D. Sumners for helpful discussions and G. Rousseau for providing numerical tools. This work was supported in part by a grant from MITACS.

[1] J. D. Murray, *Mathematical Biology* (Springer-Verlag, New York, 1989), and references herein.
[2] *Chemical Waves and Patterns*, edited by R. Kapral and K. Showalter (Kluwer Academic, Dordrecht, 1996), and references herein.
[3] J. Maselko and K. Showalter, Nature (London) **339**, 609 (1989).
[4] J. Maselko and K. Showalter, React. Kinet. Catal. Lett. **42**, 263 (1990).
[5] A. T. Winfree, *The Geometry of Biological Time* (Springer-Verlag, New York, 2001).
[6] K. M. Stein, S. M. Markowitz, S. Mittal, D. J. Slotwiner, S. Iwai, and B. B. Lerman, Chaos **12**, 740 (2002).
[7] Some aspects of cardiac arrhythmias may arise from scroll wave filament instabilities which depend on the 3D nature of cardiac tissue [8,9].
[8] A. T. Winfree, *When Time Breaks Down* (Princeton University Press, Princeton, NJ, 1987).
[9] S. Alonso, F. Sagués, and A. S. Mikhailov, Science **299**, 1722 (2003).
[10] L. Glass, Science **198**, 321 (1977).
[11] A. T. Winfree and S. H. Strogatz, Physica D **8**, 35 (1983).
[12] D. Sumners, in *Graph Theory and Topology in Chemistry*, edited by R. B. King and D. Rouvray (Elsevier, Amsterdam, 1987), p. 3.
[13] I. Cruz-White, Ph.D. thesis, Florida State University, 2003.
[14] J. G. Hocking and G. S. Young, *Topology* (Dover, New York, 1988).
[15] V. Guillemin and A. Pollack, *Differential Topology* (Prentice Hall, Englewood Cliffs, NJ, 1974).
[16] R. M. Zaritski and A. M. Pertsov, Phys. Rev. E **66**, 066120 (2002).
[17] We solve Eq. (4) numerically using an algorithm that automatically adjusts the time step to achieve an effcient simulation while controlling the error in the solution [31].
[18] V. A. Davydov, N. Manz, O. Steinbock, and S. C. Müller, Europhys. Lett. **59**, 344 (2002).
[19] It is computationally convenient to carry out the calculations in a thin spherical shell constructed from a cubic rectangular grid. The shell thickness is small compared to characteristic wavelengths and diffusion lengths so that the small shell thickness does not influence the spiral wave dynamics.

[20] The initial conditions are as in Ref. 32 with spherical coordinates $\Delta\theta=\pi/2$ and $\Delta\phi=\pi$.
[21] H. Yagisita, M. Mimura, and M. Yamada, Physica D **124**, 126 (1998).
[22] For a Gaussian distribution of β in boxes of volume 0.5^3 with mean 0.95 and standard deviation 0.013, the diameter of the spiral core meander is roughly 10 space units.
[23] A. T. Winfree, Chaos **1**, 303 (1991).
[24] V. I. Krinsky and K. I. Agladze, Physica D **8**, 50 (1983).
[25] E. A. Ermakova, V. I. Krinsky, A. V. Panfilov, and A. M. Pertsov, Biofizika **31**, 318 (1986).
[26] Y. Gong and D. J. Christini, Phys. Rev. Lett. **90**, 088302 (2003); L. Brusch, E. Nicola, and M. Bär, *ibid.* **92**, 089801 (2004).
[27] V. N. Biktashev, A. V. Holden, S. F. Mironov, A. M. Pertsov, and A. V. Zaitsev, Int. J. Bifurcation Chaos Appl. Sci. Eng. **11**, 1035 (2001).
[28] V. K. Vanag and I. R. Epstein, Science **294**, 835 (2001).
[29] V. N. Biktashev and A. V. Holden, Chaos, Solitons Fractals **5**, 575 (1995).
[30] A. S. Mikhailov, V. A. Davydov, and V. S. Zykov, Physica D **70**, 1 (1994); V. A. Davydov, V. S. Zykov, A. S. Mikhailov, and P. K. Brazhnik, Radiophys. Quantum Electron. **31**, 574 (1988).
[31] G. Rousseau and R. Kapral, Chaos **10**, 812 (2000).
[32] F. Chavez, R. Kapral, G. Rousseau, and L. Glass, Chaos **11**, 757 (2001).